frontiers | Frontiers in Physics

TYPE Mini Review
PUBLISHED 14 February 2024
DOI 10.3389/fphy.2024.1320108



OPEN ACCESS

EDITED BY
Panyu Hou,
Tsinghua University, China

REVIEWED BY
Lu Yanan,
Tsinghua University, China
Guanghui He,
Washington University in St. Louis,
United States, in collaboration with reviewer LY

*CORRESPONDENCE
Ning Wang,
ningwang@hust.edu.cn
Jianming Cai,
jianmingcai@hust.edu.cn

RECEIVED 11 October 2023
ACCEPTED 04 January 2024
PUBLISHED 14 February 2024

CITATION
Wang N and Cai J-M (2024), Hybrid quantum sensing in diamond.
*Front. Phys.* 12:1320108.
doi: 10.3389/fphy.2024.1320108



# Hybrid quantum sensing in diamond

Ning Wang[1,2]* and Jianming Cai[1,2]*

[1]International Joint Laboratory on Quantum Sensing and Quantum Metrology, School of Physics, Huazhong University of Science and Technology, Wuhan, China, [2]Hubei Key Laboratory of Gravitation and Quantum Physics, Institute for Quantum Science and Engineering, Huazhong University of Science and Technology, Wuhan, China

Quantum sensing is a quantum technology for ultrasensitive detection, which is particularly useful for sensing weak signals at the nanoscale. Nitrogen vacancy centers in diamond, thanks to their superb quantum coherence under ambient conditions and the stability of the material in extreme and complicated environments, have been demonstrated as promising quantum probes in multi-parameter sensing. Their spin properties make them particularly sensitive to magnetic fields, but they are insensitive to temperature, electric field, pressure, etc., and even immune to some bio-parameters (e.g., pH and glucose concentration). Recently, hybrid quantum sensing has emerged as a promising avenue for further enhancing the capabilities of diamond sensors. Different techniques can potentially improve the sensitivity, range of detectable parameters, and sensing frequencies of diamond sensors. This review provides an overview of hybrid quantum sensing using diamond. We first give a brief introduction to quantum sensing using diamond, and then review various hybrid sensing schemes that have been developed to enhance the sensing capabilities of diamond sensors. Finally, the potential applications and challenges associated with hybrid quantum sensing in diamond are discussed.

KEYWORDS

**quantum sensing, NV center in diamond, hybrid sensing, spin dynamics, multi-modal sensing, nanoscale sensing**

## 1 Background and introduction

Quantum sensing [1] describes the use of a quantum system, quantum properties, or quantum phenomena to perform a measurement of physical quantities. It is a new technology that can detect weak signals beyond the classical limit. It is particularly useful for sensing weak signals at the nanoscale. With unprecedented sensitivity and nanoscale resolution, quantum sensing has become a powerful probe in varieties of applications. For instance, the discovery of new materials with intriguing physical phenomena, such as van der Waals materials [2–4], topological insulators [5, 6], and complex oxide interfaces [7], has increased the need for local and non-perturbative magnetic field sensors. Such a nano-magnetometer would enable the characterization of the growing number of correlated and topological systems, as spins and moving charges generate stray fields in those systems. In addition, temperature fluctuations at the nanometer scale pose a significant role in several scenarios, including temperature-induced control of gene expression [8–10], temperature heterogeneities in living cells [11, 12], and heat dissipation in integrated circuits [13, 14]. Sensitive detection of these fluctuations is highly desirable but challenging. A thermometer with microkelvin temperature resolution, operating across a wide temperature range and offering nanoscale spatial resolution, would greatly benefit researches in physics, biology, and chemistry.

Nitrogen-vacancy (NV) centers in diamond have gained significant attention as promising quantum sensors due to their superb quantum coherence under ambient conditions and nanoscale spatial resolution. NV centers have been demonstrated to be excellent quantum magnetometers [15–17], with the ability to operate across temperatures ranging from 350 mK [18] to 1000 K [19], magnetic fields ranging from ~10 $\mu$T [20–22] to several tesla [23–25], and pressures up to 140 GPa [26, 27]. They have a dynamic sensing range that spans from direct current to gigahertz frequencies. Moreover, diamond, the host material for NV centers, offers excellent biocompatibility, the highest thermal conductivity among solids, and the stabilities in extreme environments. These characteristics are essential to NV centers in diamond as quantum probes for nanoscale sensing.

NV centers in diamond possess spin properties with unprecedented magnetic field sensitives. However, compared with magnetic field sensing, they are insensitive to other parameters, such as temperature [28–31], pressure [26], and electric field [32–34]; and even immune to many biochemical parameters (such as glucose or enzyme concentration, and pH). In order to enhance the sensitivities of parameters with a weak or even no spin response, hybrid quantum sensing has emerged. Insensitive or immune physical or biological parameters can be converted to magnetic signals and then detected by the NV center spin. This approach enables the detection and measurement of a broader range of parameters, extending the capabilities of diamond quantum sensing. Hybrid quantum sensing in diamond has already been demonstrated experimentally in recent years, showcasing the potential in multidisciplinary research.

This review focuses on recent advances on hybrid quantum sensing in diamond. We begin with an introduction to the fundamental properties and working principles of diamond quantum sensing. Hybrid sensing schemes are then discussed, with a particular emphasis on the enhanced sensitivities and broadened ranges of detectable parameters. Finally, the review finishes with outlooks for the potential applications and challenges of hybrid quantum sensing in diamond.

## 2 Brief introduction to diamond quantum sensing

NV center in diamond consists of a substitutional nitrogen atom and a vacancy [35–37] at the nearest neighborsite, as depicted in Figure 1A. When negatively charged, NV center can be treated as spin-1 system. The positively charged and neutral NV centers, however, are not of interest for quantum sensing due to the absence of magnetic resonance signals. Hereafter, all NV centers mentioned in this article refer to the negatively charged type. The energy levels of the NV center are illustrated in Figure 1B. By utilizing phonon-assisted optical absorption, the NV electron spin can be excited off-resonantly from its spin-triplet ground states to spin-triplet excited states using a 532 nm laser. The $m_s = \pm 1$ sublevels of the excited states preferentially couple to the non-radiative ISC channel, then to the singlet states, and finally to the $m_s = 0$ sublevels of the ground states. Owing to this spin-selective optical pumping process, the spin can be initialized to the $m_s = 0$ sublevel of the ground states through continuous optical cycling. Consequently, the intensity of photoluminescence when the NV center is at the ground states $m_s = \pm 1$ sublevels is ~30% lower than that of sublevel $m_s = 0$, allowing distinguishing the $m_s = 0$ spin state from $m_s = \pm 1$ states at room temperature.

The Hamiltonian of the ground states of an NV center gives the sensing principle and is written as

$$H = \left(D_{gs} + k_{gs}^{\parallel}\Pi_z\right)S_z^2 - k_{gs}^{\perp}\Pi_x\left(S_xS_x - S_yS_y\right) + k_{gs}^{\perp}\Pi_y\left(S_xS_y + S_yS_x\right) + \gamma_e \boldsymbol{B}\cdot\boldsymbol{S}, \tag{1}$$

where $D_{gs} = 2.87$ GHz is the zero-field splitting at ground states; $\boldsymbol{S}$ is the spin-1 Pauli operator, $\gamma_e = 2.802$ MHz/Gauss is the

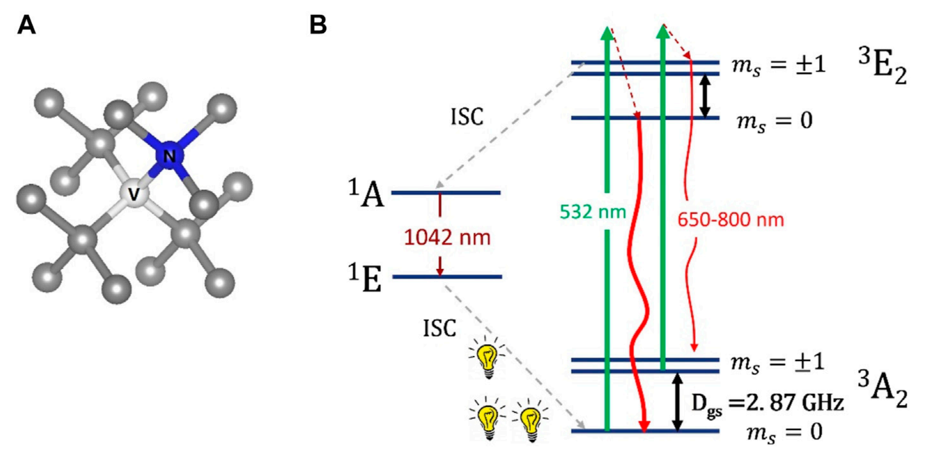


FIGURE 1
Nitrogen-vacancy (NV) center in diamond. **(A)** The atomic structure of NV center in diamond. The NV center consists of a substitutional nitrogen and a nearby vacancy. **(B)** Energy levels of an NV center. The spin is pumped into $m_s = 0$ by continuous excitation, and the $m_s = \pm 1$ excited states can decay through metastable singlet states. The spin states can be optically detected by spin-dependent photoluminescence as $m_s = 0$ state is brighter than $m_s = \pm 1$ states.

**TABLE 1 Summary of the filter functions, sensing frequencies, and sensitivity for the three types of sensing protocols. For the transverse spin relaxation measurements, Ramsey, spin echo and CPMG-N (N is the number of the flip pi pulse) are listed as examples. $\omega_0$, NV spin resonance frequency; $\Gamma = 1/T_2^*$, NV dephasing time; $t_d$ free evolution time; $t_{acq}$, acquisition time; $t_\pi$, the $\pi$-pulse length; c, the normalization constant. upper sign for even $N$ and lower sign for odd $N$ in the filter equation of CPMG-N.**

| Protocols | Filter function [1, 42–44] | Sensitive to $B_\parallel$ with typical frequency | Sensitive to $B_\perp$ with typical frequency | Typical sensitivity |
|---|---|---|---|---|
| ODMR | $\frac{1}{c}$ when $\frac{2\pi}{t_{acq}} < \omega < \frac{2\pi}{t_\pi}$ 0, otherwise | $10^{-3}$–$10^{1}$ Hz | . . .[a] | ~ $\mu T/\sqrt{Hz}$ [16, 17, 45] |
| Ramsey | $\mathrm{sinc}^2 \frac{\omega t_d}{2}$ | $10^{-3}$–$10^{5}$ Hz | . . .[a] | ~ $\mu T/\sqrt{Hz}$ [16, 17, 45] |
| Spin echo | $\frac{1}{2}\mathrm{sinc}^2 \frac{\omega t_d}{4}$ | $10^{3}$–$10^{6}$ Hz | | ~ $nT - pT/\sqrt{Hz}$ [16, 17, 46, 47] |
| CPMG-N | $2\frac{\sin^2\frac{\omega t_d}{4N}}{\cos^2\frac{\omega t_d}{2N}} \frac{1 \mp \cos \omega t_d}{(\frac{\omega t_d}{2})^2}$ | $10^{4}$–$10^{7}$ Hz | | |
| $T_1$ relaxometry | $\frac{1}{\pi}\frac{\Gamma}{\Gamma^2+(\omega-\omega_0)^2}$ | | $\omega_0$ (~ GHz) | |

[a]Also affected by $T_1$ relaxation.

gyromagnetic ratio of the electron spin; $\boldsymbol{B}$ is the magnetic field applied on the NV center; $k_{gs}^{\parallel} = 0.35 \pm 0.02\,\mathrm{Hz\,cmV^{-1}}$ and $k_{gs}^{\perp} = 17 \pm 3\,\mathrm{Hz\,cmV^{-1}}$ are the parallel (axial) and the transverse (nonaxial) components of electric-field coupling strengths [32], respectively. Given that crystal strain [38–40] can be treated effectively as a local static electric field $\boldsymbol{\sigma}$, it combines with the external electric field $\boldsymbol{E}$ to give the total effective field $\boldsymbol{\Pi}(\Pi_x, \Pi_y, \Pi_z) = \boldsymbol{E} + \boldsymbol{\sigma}$ at the NV center.

NV centers are primarily sensitive to magnetic fields, as manifested in the Zeeman term of Eq. 1 with a coupling strength $\gamma_e = 2.8$ MHz/Gauss. NV centers are responsive to magnetic noise in a wide frequency range, from direct current up to ~100 GHz [23–25]. There are three main magnetic sensing protocols. The first one is continuous-wave optically detected magnetic resonance (ODMR) measurement. The energy level difference between the $m_s = -1$ and $m_s = +1$ sublevels is lifted by $2\gamma_e B_z$ ($B_z$ is the magnitude of the axial magnetic field). By continuously polarizing the spin states with a 532 nm laser and sweeping the microwave frequencies, the resonant frequencies $\omega_\pm = D_{gs} \pm \gamma_e B_z$ can be obtained. The second protocol is based on transverse spin relaxations, which involves preparing a superposition state, periodically flipping its phase using microwave $\pi$ pulses, then coding the accumulated phase to spin population by an additional $\pi/2$ pulse, and finally reading out the spin population through photoluminescence (such as spin echo measurements, CPMG sequences and other dynamical decoupling methods [41–43]). It is sensitive to magnetic fields at the spin-flip frequency. The third protocol is longitudinal spin relaxation ($T_1$ relaxometry), where a spin eigenstate is prepared and the spin population is monitored as a function of time. NV $T_1$ relaxometry is sensitive to magnetic field power spectra density $g(\omega_\pm)$, where $\omega_\pm$ are the resonant frequencies between $m_s = 0$ and $m_s = \pm 1$. Furthermore, by tuning the external magnetic field, the final technique makes NV centers capable of sensing magnetic noise at frequencies up to 100 GHz [23–25]. The filter functions, sensing-frequency ranges, and together with sensitivities of the three types of protocols are summarized in Table 1.

NV centers are also responsive to temperature, pressure, and electric fields, although the sensitivity is much lower than magnetic fields. The zero-field splitting $D_{gs}$ is related to the structural distortions that can affect the dipole-dipole coupling, which can be induced by temperature changes and pressure. The corresponding responses to temperature and pressure changes are -74 kHz/K [28] and 14.58 (6) MHz/GPa [26], respectively. When an electric field is applied, NV center also shows shifts in energy levels due to the stark effect [32]. However, the electric-field coupling strength $k_{gs}^{\perp}$ and $k_{gs}^{\parallel}$ [32] are much smaller than the magnetic-field coupling, leading to rather low sensitivity of the electric field. Despite low sensitivities to theses parameters, NV sensors have advantages such as high thermal diffusivities, and stability in bio-environments or extreme environments which are desirable for thermal characterizations, or *in vivo* monitoring of living organisms, etc. Therefore, developing methods for improving the sensitivity to multiple physical parameters is crucial.

# 3 Hybrid diamond quantum sensing

Hybrid sensing is a strategy for accurately measuring insensitve parameters by detecting a different parameter to which the NV center is highly sensitive [48]. This section reviews recent advances in hybrid sensing using NV centers in diamond, for measurement of temperatures, pressure, and bio-parameters, as well as further boosted sensitivity to magnetic fields compared with pristine NV centers.

## 3.1 Temperature sensing

NV thermometry has been attractive for the past 10 years due to its nanoscale spatial resolution, high thermal diffusivity (fast thermal response), and the wide working temperature ranges from cryogenics to 1000 K. In particular, the good bio-compatibility also ensures its application in probing thermal behaviors in biological systems [31, 49–51]. The temperature response of NV centers was first reported in 2010 [28]. The zero-field splitting $D_{gs}$ decreases with the increasing temperature with the coefficient of −74 kHz/K. Various temperature sensing protocols are then proposed, including delicate design of pulse sequences [29–31] for precise measurement of the temperature-dependent $D_{gs}$, as well as all-optical methods that characterizes the fluorescence spectroscopy without microwave modulations [52, 53]. Based on these thermometry protocols, NV in diamond has been successfully applied for *in situ* monitoring the thermal behavior of living systems [31, 49–51]. Typically, the sensitivity to temperature of a single NV

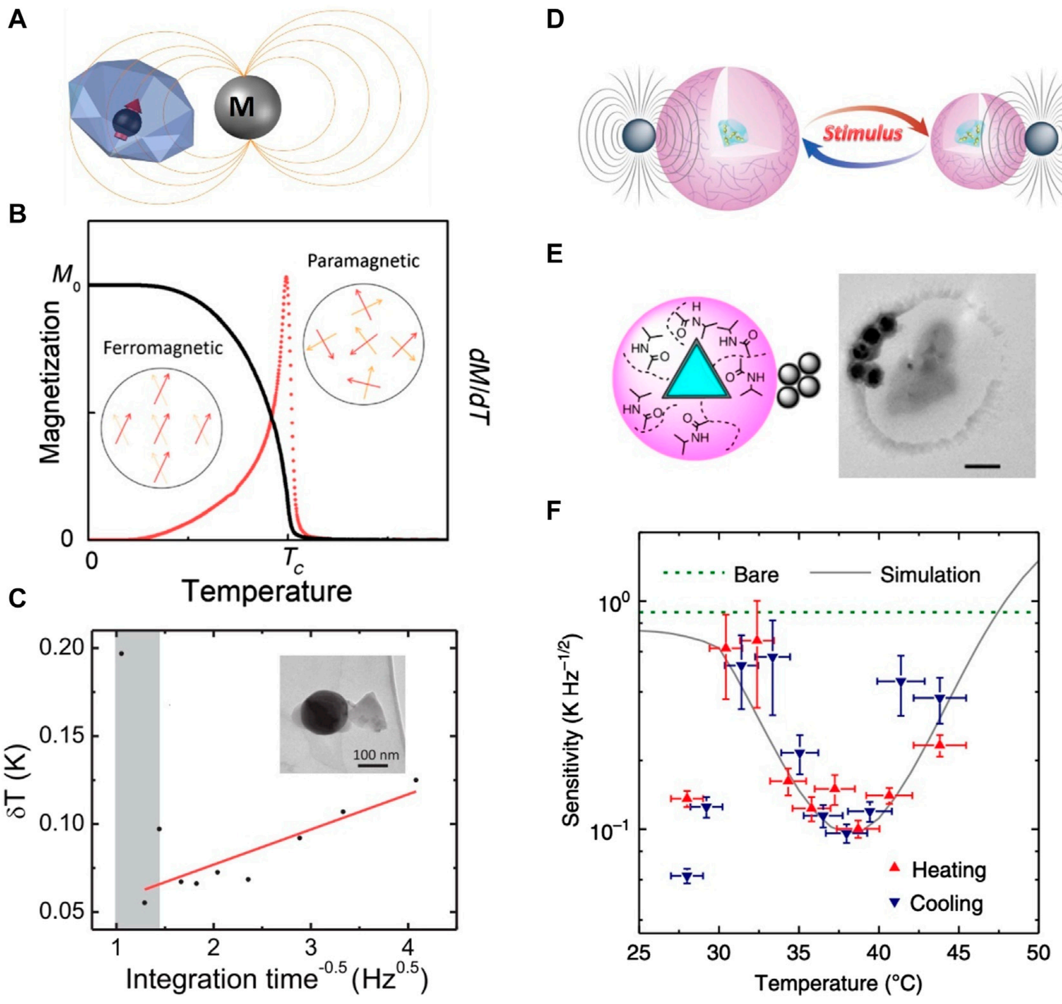


FIGURE 2
Hybrid diamond nano-thermometry. **(A)** Schematic of a hybrid nanosensor, composed of a fluorescent nanodiamond and a magnetic nanoparticle (MNP). **(B)** The magnetic moment M (black solid line) of the MNP decreases dramatically with temperature increasing to the ferromagnetic-paramagnetic transition, with the temperature susceptibility dM/dT (red dotted line) peaking at the critical temperature $T_C$. The transition frequencies of the NV center spin in the nanodiamond depend sensitively on the magnetic moment of the MNP and hence the temperature. **(C)** The temperature sensitivity measured experimentally by three-point ODMR measurements. The inset is the transmission electron microscopy (TEM) image of the hybrid system. Reproduced from Ref. [54] with permission from [APS], Copyright [2018]. **(D)** Schematic of an ND@hydrogel–MNP hybrid sensor. **(E)** Chemical structure illustration and TEM image of the hybrid sensor. **(F)** Sensitivities of the ND@pNIPAM–Ni hybrid sensor. Reproduced from Ref. [55] with permission from [Nature], Copyright [2018].

center in bulk diamond with $^{13}$C natural abundance is on the order of several $\mathrm{mK}/\sqrt{\mathrm{Hz}}$. Unfortunately, there is a trade-off between temperature sensitivity and spatial resolution. For example, when using NV centers in nanodiamonds, the temperature sensitivity is only $130\,\mathrm{mK}/\sqrt{\mathrm{Hz}}$ due to the shorter coherence time, even with delicate design of pulse sequences and optimized experimental conditions (e.g., optimized laser power, microwave intensity, and photoluminescence collection efficiency). Probing temperature in living systems is even more challenging because strong laser and microwave excitations are not feasible, and the sensitivity is reduced to approximately $\sim \mathrm{K}/\sqrt{\mathrm{Hz}}$ [50, 51].

Hybrid schemes have been proposed and demonstrated to improve the sensitivity of temperature sensing by using magnetic nanoparticles (MNPs). Two hybrid schemes have been proposed and demonstrated, both of which convert temperature variations into magnetic field changes that can be detected by NV centers. The first scheme is based on magnetic criticality enhancement [54]. In this configuration, a single $Cu_{1-x}Ni_x$ alloy MNP is combined with a nanodiamond containing ensemble NV centers, as illustrated in Figure 2A. The magnetization of the MNP can be used to monitor the local temperature, and this mechanism becomes highly sensitive when the temperature is close to the magnetic phase transition point (i.e., critical point) of the MNP, as shown in Figure 2B. This results in a sensitivity of $11\,\mathrm{mK}/\sqrt{\mathrm{Hz}}$ under ambient conditions [Figure 2C], which marks a significant step forward compared to the previous sensitivity record of $130\,\mathrm{mK}/\sqrt{\mathrm{Hz}}$ without hybrid sensing. By using a single NV in a diamond pillar that can provide both bright photon counts and long coherence time, it is predicted that the sensitivity can be further improved to $\sim \mu\mathrm{K}/\sqrt{\mathrm{Hz}}$ [54]. Later experimental demonstrations using diamond nanopillars achieved a sensitivity of $\sim 76\,\mu\mathrm{K}/\sqrt{\mathrm{Hz}}$ [56]. This strategy by converting temperature variations to magnetization signals is also

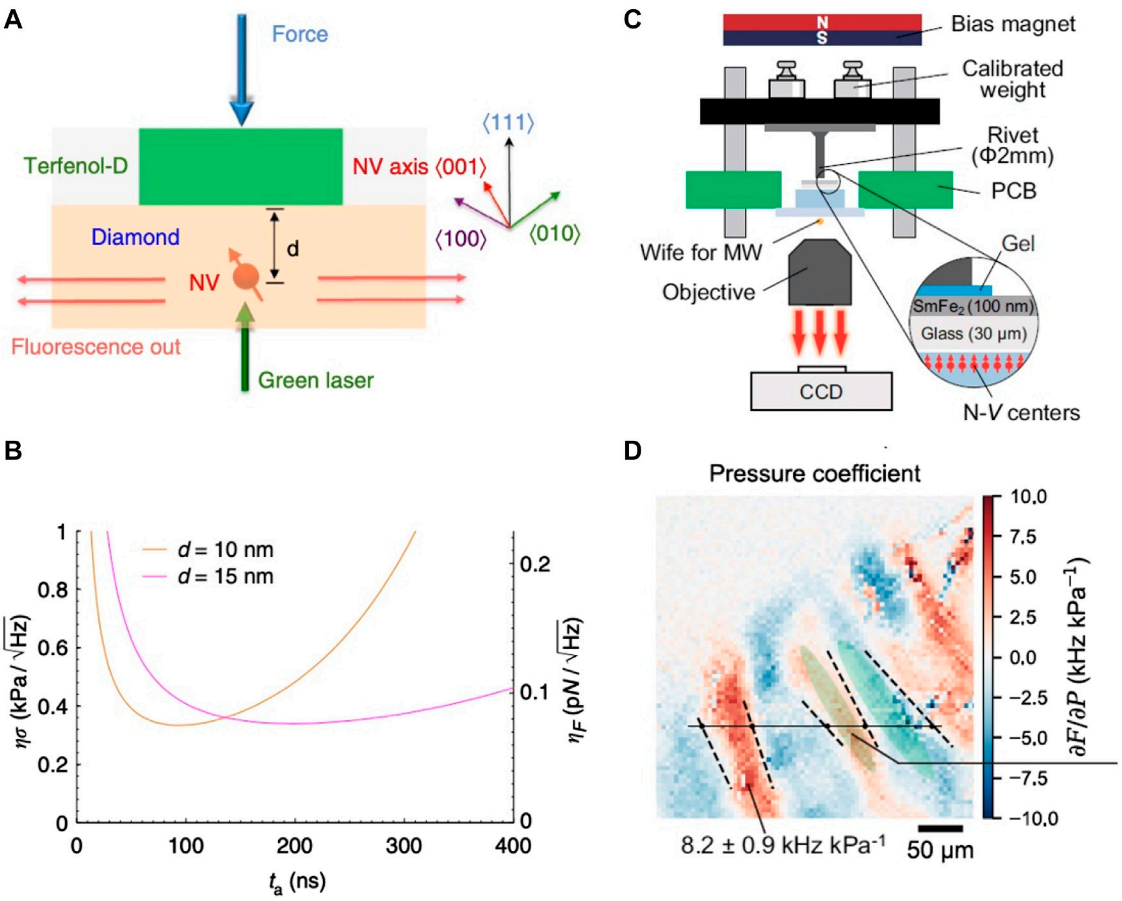


FIGURE 3
Hybrid diamond pressure sensing. **(A)** The model hybrid system of diamond (brown) and piezomagnetic film (green). **(B)** Simulation results of the shot-noise-limited sensitivity for the measurement of stress (and force) as a function of the integration time ($t_a$, free evolution time in Ramsey measurement chosen for sensing, details in Ref. [58]). The yellow and purple lines are the simulation results for $d$ = 10 nm and $d$ = 15 nm respectively, where $d$ is the distance between the NV center and piezomagnetic film as illustrated in **(A)**. Reproduced from Ref. [58] with permission from [Nature], Copyright [2014]. **(C)** Experimental setup for imaging the magnetic response to external magnetic field using the hybrid structure. Pressure is applied by calibrated weight through a rivet with a diameter of 2 mm into $SmFe_2$. Gel is placed between the $SmFe_2$ layer (100 nm) and foot of the rivet to homogenize the pressure. The distance between the NV centers and the $SmFe_2$ layer is at least 30 μm. CCD camera is used to images the photoluminescence from NV centers. **(D)** Distribution of the pressure coefficient. Maximum pressure coefficient is (8.2 ± 0.9) kHz/kPa. Reproduced from Ref. [59]with permission from [APS], Copyright [2023].

implemented in a fiber sensor based on bulk diamond coupled to a permanent magnet, with a sensitivity of 1.6 mK/$\sqrt{\text{Hz}}$ [57].

The second scheme involves the use of both MNPs and a functional hydrogel [55], as depicted in Figures 2D, E. In this configuration, a stimulus-responsive hydrogel acts as a spacing transducer between a nanodiamond with NV centers and MNPs. The volume phase transition of the hydrogel, triggered by temperature stimulation, leads to a sharp variation in the separation distance between the MNPs and nanodiamonds. This results in a magnetic field change that can be detected by NV centers. Using this scheme, a temperature sensitivity of 96 mK/$\sqrt{\text{Hz}}$ has been achieved, as shown in Figure 2F. These schemes demonstrate the potential for improving the sensitivity to temperature through hybrid sensing.

Both of these methods rely on thermally responsive phase changes to achieve high sensitivity to temperature. However, sensing range of temperature is limited by the phase change point and dynamics. In the case of the magnetic criticality enhanced hybrid nano-thermometer, the working temperature range is within ~20 K below the Curie temperature. Although the working range can be increased by applying an external magnetic field, it will compromise the temperature sensitivity as the magnetic susceptibility becomes less responsive to temperature under external magnetic field. The limited sensing range can be mitigated by tuning the Curie temperature of magnetic nanoparticles through alloying to meet the requirement of different scenarios. For example, the Curie temperature of the copper-nickel magnetic nanoparticles can be continuously tuned from 4 K to 600 K by manipulating the nickel composition [54]. For hybrid sensing based on volume phase changes of hydrogels, the working range is within only ±7 K near the critical temperature [55]. The utilization of hydrogel also limits the applications in higher temperature sensing due to the solvent evaporation.

## 3.2 Pressure sensing

Hybrid sensing schemes have also been proposed and demonstrated to improve the sensitivity of pressure and force

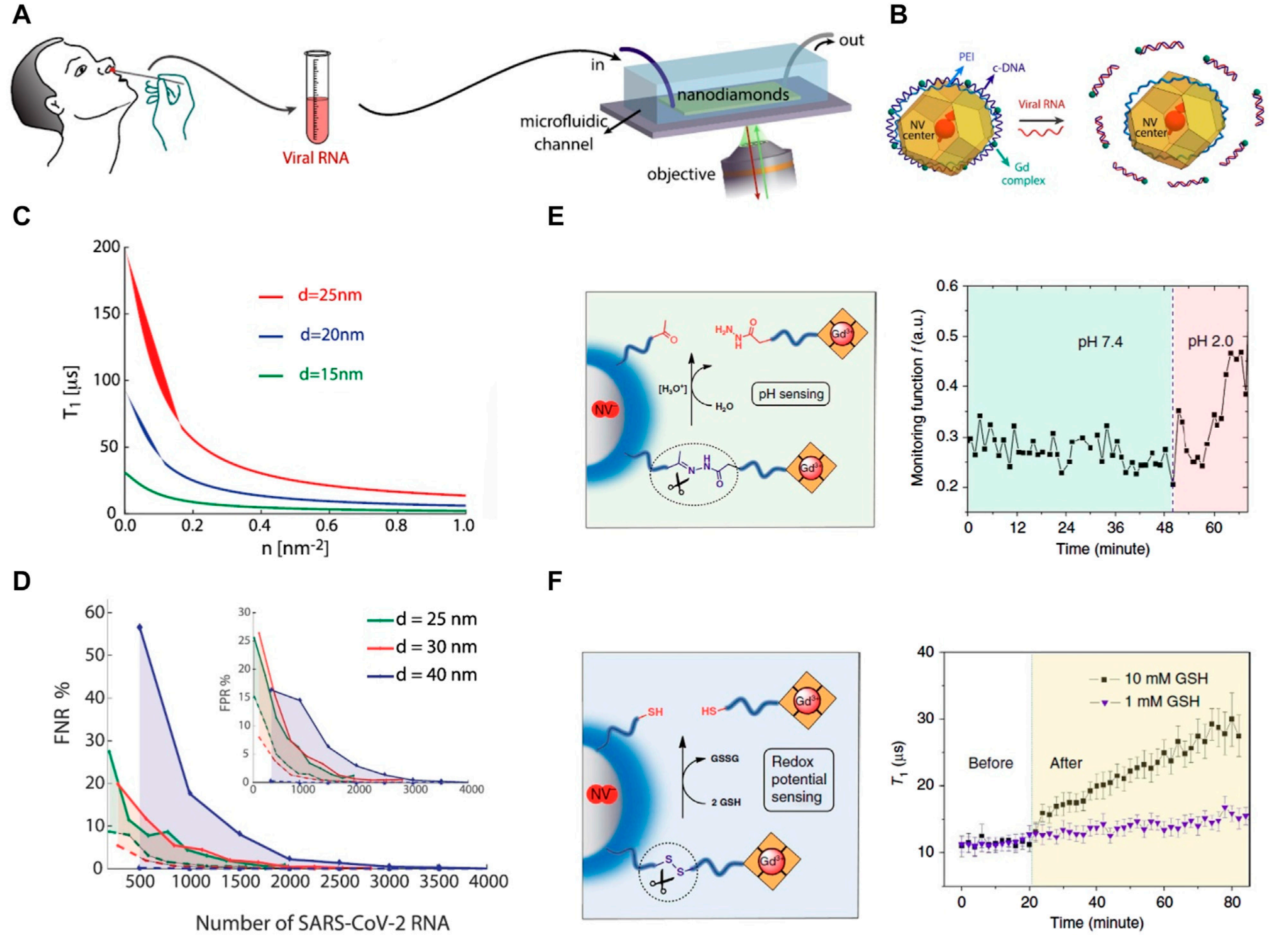


FIGURE 4
Hybrid diamond bio-sensors. **(A)** Overview of the diagnosis protocols. **(B)** Mechanism of magnetic noise quenching. In the presence of virus RNA, the base-pair matching of c-DNA and RNA leads to the detachment of c-DNA-DOTA-$Gd^{3+}$ from the nanodiamond surface, resulting in weaker magnetic interaction between $Gd^{3+}$ complex and NV centers inside the nanodiamond. **(C)** Simulation of relaxation time $T_1$ as a function of the surface density of $Gd^{3+}$ complex molecules. Here is the performance of a single NV center at the center of a single ND with diameter $d$ ($d$ = 15, 20, 25 nm respectively). **(D)** FNR (inset: FPR) as a function of the number of SARS-CoV-2 RNA copies associated with ensemble NDs (5,000 NDs with one NV each and the NV position is random in a sphere of 20% of the ND radius, and the average surface c-DNA-DOTA-$Gd^{3+}$ density is 0.1 $nm^{-2}$) with different diameters $d$ ($d$ = 25, 30, 40 nm respectively). The solid (dashed) curves show the worst (optimal) case. Reproduced from Ref. [60] with permission from [ACS Publications], Copyright [2022]. **(E)** pH-sensors sensing mechanism and NV response (time-dependent fixed $\tau$ measurements) to pH changes. **(F)** Redox-sensors sensing mechanism and NV response ($T_1$ measurement) to redox changes. Reproduced from Ref. [61] with permission from [Nature], Copyright [2017].

sensing using diamond. One approach is to deposit a piezomagnetic film, such as $Tb_{0.27}Dy_{0.73}Fe_2$ (Terfenol-D), onto a bulk diamond as a signal transducer, as shown in Figure 3A [58]. The piezomagnetic film exhibits high magnetostrictive effects, allowing the external stress to be converted into a magnetic field change. Simulation results show that the sensitivity for measuring stress (and force) can reach 0.35 kPa/$\sqrt{\mathrm{Hz}}$ (tens of fN/$\sqrt{\mathrm{Hz}}$) under ambient conditions with state-of-the-art experimental capabilities, as shown in Figure 3B. Recently, an experimental work demonstrated a hybrid sensing scheme for pressure and force using a combination of in-plane magnetized $SmFe_2$ as a magnetostrictive (MS) layer and diamond with [111]-oriented NV centers [59], depicted in Figure 3C. This configuration enables the detection of pressure-to-magnetic field conversion. The achieved pressure coefficient approaches 8.2 kHz/kPa, which is 500 times greater than that of bare NV centers, as shown in Figure 3D, almost comparable with the simulated coefficient of about 10 kHz/kPa reported in Ref. [58].

However, there remain some issues to be addressed for applications. For instance, the pressure coefficient is correlated with magnetic domain structures, as shown in Ref. [59]. This correlation could lead to an inhomogeneous pressure response in wide-field pressure imaging, which requires complicated calibration efforts. The authors also proposed that using magnetic disk arrays could potentially address these issues, which could be explored in future research [59].

## 3.3 Bio-parameter sensing

Hybrid sensing can enable accurate detection of bio-parameters which NV centers show no spin response. A recent theoretical work

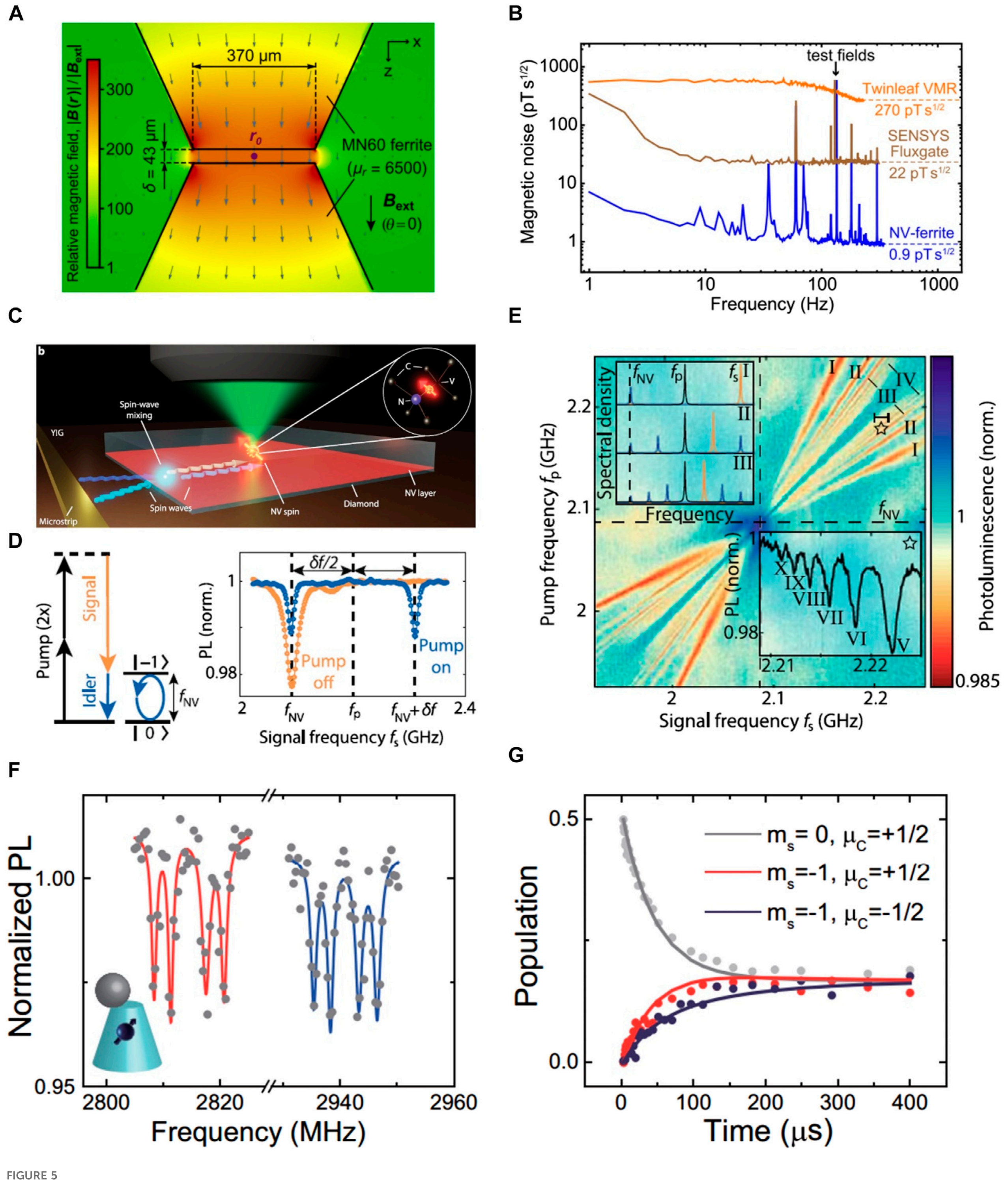


FIGURE 5
Hybrid schemes to enhance magnetic field sensing. **(A)** MFC structures is combined with ensemble NVs in bulk diamond. The magnetic material here is MN60 ferrite with a permeability of $\mu_r = 6500$. **(B)** A comparison of the magnetic noise spectra of a commercial magnetoresistive magnetometer (Twinleaf VMR), flux-gate magnetometer (SENSYS FGM-100) and the NV-MFC (ferrite) magnetometer shown in **(A)** with dual-resonance measurement. The measured highest magnetic field sensitivity of NV-MFC magnetometer is 0.9 pT/Hz$^{1/2}$. Reproduced from Ref. [64] with permission from [APS], Copyright [2020]. **(C)** Sketch of the setup. A diamond with implanted 10–20 nm NV centers is placed onto a film of yttrium iron garnet (YIG, thickness 235 nm). The signal and pump microwaves are delivered through the microstrip to excite spin waves in YIG. The spin-wave mixing enables detection of the signal field by converting its frequency to the NV electron spin resonance frequency. **(D)** Energy diagram of four-wave mixing and the normalized NV PL vs. $f_s$. **(E)** Spin-wave comb observed in the PL versus $f_s$ and $f_p$. Upper inset: Spectrum to illustrate the detection of the idlers I-III (black: pump, orange: signal, blue: idlers). Lower inset: Linecut along the black line at the star in the main panel, showing idlers up to the tenth order. Reproduced from Ref. [66] with permission from [Nature], Copyright [2023]. **(F)** ODMR spectrum of a single NV center coupled to a nearest $^{13}$C nuclear spin with a magnetic nanoparticle placed in the proximity. **(G)** Populations in the states $|m_s = -1, \mu_C = +\frac{1}{2}\rangle$ (red), $|m_s = -1, \mu_C = -\frac{1}{2}\rangle$ (navy), and $|m_s = -1, \mu_C = +\frac{1}{2}\rangle$ (gray) as

*(Continued)*

FIGURE 5 (Continued)
functions of the time after initialization. The strong hyperfine coupling enabling sensing noise frequencies around the transition frequencies 2.870 $\pm \gamma_e B_z \pm$ 0.065 GHz. The transition rates between different states can be obtained from the spin populations through rate equation, details for the deduction are in Ref. [20]. Reproduced from Ref. [20].with permission from [APS], Copyright [2022].

proposed that $T_1$ relaxometry can be used to detect RNA of SARS-CoV-2 from magnetic fluctuations from magnetic species like the $Gd^{3+}$ ion complexes [60], as shown in Figure 4A. In this proposed scheme, functionalized nanodiamonds containing NV centers coated with cationic polyethyleneimine (PEI) polymers are loaded into microfluidic channels containing solution to be tested, as shown in Figure 4B. When there are no SARS-CoV-2 RNA molecules in the liquid, the $Gd^{3+}$ complexes remain attached to the c-DNA on the functionalized diamond surfaces, and a strong magnetic noise can be detected by $T_1$ relaxometry. In contrast, the presence of RNA would lead to the detachment of c-DNA-DOTA-$Gd^{3+}$ from the nanodiamond surface, resulting in weaker magnetic signals. Considering a single NV center in the center of a nanodiamond with a diameter $d$, the simulation results of relaxation $T_1$ as a function of the surface density of $Gd^{3+}$ complex molecules are presented in Figure 4C, where the presence of RNA corresponds to a low density of $Gd^{3+}$ complex molecules and *vice versa*. To enhance the sensitivity, an ensemble of NDs is used to increase the signal-to-noise ratio. This method is predicted to have a sensitivity down to a few hundred RNA copies with a false negative rate (FNR; false positive rate, FPR) of less than 1%, as shown in Figure 4D [60] which is the result of 5,000 NDs with one NV in each. Similar protocols can also be used to monitor changes in pH or redox potential at the sub-micron scale using microfluidic channels that mimic cellular environments [61, 62]. By attaching paramagnetic gadolinium complexes to nanodiamonds through surface engineering, their responses to pH and redox changes can be effectively measured, as shown in Figures 4E, F [61], respectively. Overall, combining functionalized nanodiamonds and magnetic species can serve as a general hybrid sensing platform with potential applications ranging from catalytic chemistry to cell biology and physiology. However, these sensors are one-time indicators that cannot perform several measurements without replacement, which limits their application in real-time monitoring of bio-signals.

## 3.4 Ultrasensitive magnetic field sensing

Hybrid sensing strategies can further enhance the sensitivity to magnetic fields. For example, the sensitivity to magnetic field can be dramatically enhanced by placing a ferromagnetic (FM) particle between the NV center and a target spin. In this theoretically proposed scheme, the target spin resonantly drives magnetization of the FM particle, which can be regarded as a macrospin that amplifies signal detected by the NV center. The magnetic sensitivity is potentially capable of detecting a single nuclear spin with milliseconds of data acquisition [63]. Another approach is to combine NV centers with magnetic flux concentrators (MFCs) with high magnetic permeability to magnify the magnetic fields [64, 65], as shown in Figure 5A. The measured sensitivity can reach 0.9 $\mathrm{pT}/\sqrt{\mathrm{Hz}}$ as shown in Figure 5B [64]. By optimizing the geometry of MFCs and using ensemble NVs, magnetic field sensitivity can be further improved to $(196 \pm 60)\ \mathrm{fT}/\sqrt{\mathrm{Hz}}$ [65]. However, improved sensitivity using MFCs compromises the spatial resolution of the NV probes, and miniaturization of MFCs is necessary.

In addition, the sensing frequency range of NV centers in microwave regimes can be broadened through hybridization with other systems, such as nuclear spins, thin film magnets, and others. Current literature mainly relied on the tuning of electron spin resonance frequencies using a bias field for manipulating the sensing frequency range. However, the bias field can affect the properties such as permeability, magnetic domain structures, and others, of the samples. To address this, one approach is to interface NV centers in diamond with a thin-film magnet [66]. By applying a local pump field, microwave signals can be converted to the NV spin frequency via the non-linear spin-wave dynamics of the magnet, as shown in Figures 5C, D. This allows for the detection of microwave signals that are detuned by several GHz from the NV resonance frequency, enabling the characterization of spin-wave band structures and non-linear spin-wave dynamics, as shown in Figure 5E. Another approach is to couple NV centers with $^{13}C$ nuclear spins [20]. This coupling can enable multi-frequency sensing at microwave frequencies. By manipulating the states of both the NV center and the $^{13}C$ nuclear spins, it is possible to probe and measure different frequencies simultaneously, as shown in Figures 5F, G. These hybridization techniques open up new possibilities for NV centers to be used as versatile quantum sensors in a wider range of frequencies and applications.

Finally, hybrid sensing can also be achieved by coupling NV centers with surface quantum excitations. For example, the photoluminescence of NV centers can be largely boosted by coupling NV centers to gold/silver plasmonic nanostructures [67, 68]. The microwave-spin interaction can also be enhanced by coupling NV centers with surface magnons by employing focused electromagnetic fields using a hybrid nanowire-bowtie antenna [69].

# 4 Opportunities and challenges

Hybrid sensing significantly enhances the sensing capabilities of NV centers in diamond (a comparison between bare NV sensing and hybrid NV sensing is summarized in Table 2), opening up exciting possibilities for advancing diamond quantum sensing applications. Among these, precise nanoscale temperature sensing emerges as a particularly promising avenue. Given the tight thermoregulation of cellular compositions, gaining insights into temperature variations within living cells is imperative for unraveling the mechanisms governing temperature-dependent biological processes. The hybrid nanothermometer, leveraging magnetic criticality enhancements, offers an impressive boost in sensitivity up to two

TABLE 2 A comparison between bare NV sensing and hybrid sensing for different sensing parameters. For magnetic field sensing, only sensing frequency around GHz is listed and compared.

| Sensing parameter | Bare NV sensing | | Hybrid NV sensing | |
|---|---|---|---|---|
| | Coupling coefficient | Sensitivity/Frequency | Coupling coefficient | Sensitivity/Frequency |
| Temperature | $\partial D/\partial T$ [28] (−74 kHz/K) | ~ mK/$\sqrt{\text{Hz}}$ [29–31] (single NV in bulk) | $\partial B/\partial T$ (14/47 MHz/K) [54, 56] | ~ $\mu$K/$\sqrt{\text{Hz}}$ [54, 56] (single NV in bulk) |
| | | 130 mK/$\sqrt{\text{Hz}}$ [29] (nanodiamonds) | | 11 mK/$\sqrt{\text{Hz}}$ [54] (nanodiamonds) |
| Pressure | $\partial D/\partial P$ [26] (14.5 Hz/kPa) | 0.60 MPa/$\sqrt{\text{Hz}}$ [26] | $\partial B/\partial P$ [58, 59] (10 kHz/kPa) | 0.35 kPa/$\sqrt{\text{Hz}}$ [58] |
| Bio-parameter (X) | no spin response | | spin response [60–62] ($\partial B/\partial X$) | |
| Magnetic field | $\gamma_e$ (2.8 GHz/T) | ~ $\mu$T/$\sqrt{\text{Hz}}$ (dc) [16, 17, 45]/$\omega_0$ sensing around GHz | $\gamma_e$ (2.8 GHz/T) | ~ 0.2 pT/$\sqrt{\text{Hz}}$ (dc) [65]/Multi frequencies sensing around GHz [20, 66] |

orders of magnitude, which is promising for resolving the long-standing controversies in understanding temperature heterogeneities within living cells. By choosing magnetic nanoparticles with Cuire temperatures around 37°C, the working temperature range of hybrid sensors can be used for *in vivo* thermal characterizations of living cells, although the calibration can be complicated. One possible approach to solving the aforementioned challenge is to conduct the *in vivo* measurement and then perform the calibration after the death of the cell, which involves real-time three-dimensional tracking of the sensors [70, 71].

Hybrid sensing opens up the possibilities of using quantum probes for understanding bio-processes in the future. In microreactors such as living cells, hybrid quantum sensors can be used to study the nanoscale variations in pH and concentration of species playing a pivotal role in biochemical reactions, such as ATP synthesis and the release or consumption of neurotransmitters. However, many reported hybrid bio-sensors are one-time indicators as discussed above, and developing sensors that can achieve real-time monitoring of bio-signals can be a fruitful direction.

As for sensing magnetic fields, the enhanced sensitivities achieved with NV diamond quantum sensors and MFCs are approaching to those of established technologies like superconducting quantum interference devices and atomic vapor-based sensors. However, the spatial resolution is also reduced at the same time when MFCs are introduced. In principle, miniaturizing the MFC could potentially improve spatial resolution to some extent. However, the enhancement factor depends on the magnetic permeability of the material and the geometry of the MFCs. Therefore, search for magnetic materials with suitable permeability and the optimization of the MFC design geometry should be paid enough attention in future researches. This enhanced magnetic field sensitivity opens up possibilities of future applications in precision navigation, geoscience, and medical imaging, where accurate detection and measurement of magnetic fields are crucial.

Although this article is focused on NV centers in diamond, the hybrid sensing schemes summarized in this review can also be used in other defects in solids as well, such as SiV [72, 73] and GeV [74, 75] in diamond, SiV [76, 77]and divacancy centers [78, 79] in silicon carbide, and defect centers in 2D materials [80–82].

To conclude, past decade witnessed rapid progresses in developing hybrid quantum sensors, and we expect hybrid quantum sensing will impact multidisciplinary research in fields such as non-equilibrium thermodynamics in bio-systems, heat dissipation in nanodevices, and bio-signal detection in disease diagnostics, and many others. Furthermore, future practical implementation and commercialization of quantum hybrid sensors require interdisciplinary efforts, involving techniques in quantum information science, condensed matter physics, and technology for sensor development, as well as expertise from various other fields (biology, chemistry, engineering, etc.).

## Author contributions

NW: Conceptualization, Resources, Writing–original draft, Funding acquisition; JC: Conceptualization, Resources, Writing–review and editing, Funding acquisition.

## Funding

The author(s) declare financial support was received for the research, authorship, and/or publication of this article. This work was supported by the National Natural Science Foundation of China (12304571, 12161141011).

## Conflict of interest

The authors declare that the research was conducted in the absence of any commercial or financial relationships that could be construed as a potential conflict of interest.

## Publisher's note

# References


1. Degen CL, Reinhard F, Cappellaro P. Quantum sensing. *Rev Mod Phys* (2017) 89: 035002. doi:10.1103/RevModPhys.89.035002

2. Gong C, Zhang X. Two-dimensional magnetic crystals and emergent heterostructure devices. *Science* (2019) 363:eaav4450. doi:10.1126/science.aav4450

3. Huang B, Clark G, Navarro-Moratalla E, Klein DR, Cheng R, Seyler KL, et al. Layer-dependent ferromagnetism in a van Der Waals crystal down to the monolayer limit. *Nature* (2017) 546:270–3. doi:10.1038/nature22391

4. Gong C, Li L, Li Z, Ji H, Stern A, Xia Y, et al. Discovery of intrinsic ferromagnetism in two-dimensional van Der Waals crystals. *Nature* (2017) 546:265–9. doi:10.1038/nature22060

5. Hasan MZ, Kane CL. Colloquium: topological insulators. *Rev Mod Phys* (2010) 82: 3045–67. doi:10.1103/revmodphys.82.3045

6. Soumyanarayanan A, Reyren N, Fert A, Panagopoulos C. Emergent phenomena induced by spin–orbit coupling at surfaces and interfaces. *Nature* (2016) 539:509–17. doi:10.1038/nature19820

7. Hwang HY, Iwasa Y, Kawasaki M, Keimer B, Nagaosa N, Tokura Y. Emergent phenomena at oxide interfaces. *Nat Mater* (2012) 11:103–13. doi:10.1038/nmat3223

8. Kamei Y, Suzuki M, Watanabe K, Fujimori K, Kawasaki T, Deguchi T, et al. Infrared laser–mediated gene induction in targeted single cells *in vivo*. *Nat Methods* (2009) 6: 79–81. doi:10.1038/nmeth.1278

9. Lauschke VM, Tsiairis CD, François P, Aulehla A. Scaling of embryonic patterning based on phase-gradient encoding. *Nature* (2013) 493:101–5. doi:10.1038/nature11804

10. Kumar SV, Wigge PA. H2A.Z-Containing nucleosomes mediate the thermosensory response in arabidopsis. *Cell* (2010) 140:136–47. doi:10.1016/j.cell.2009.11.006

11. Kiyonaka S, Sakaguchi R, Hamachi I, Morii T, Yoshizaki T, Mori Y. Validating subcellular thermal changes revealed by fluorescent thermosensors. *Nat Methods* (2015) 12:801–2. doi:10.1038/nmeth.3548

12. Baffou G, Rigneault H, Marguet D, Jullien L. A critique of methods for temperature imaging in single cells. *Nat Methods* (2014) 11:899–901. doi:10.1038/nmeth.3073

13. Mecklenburg M, Hubbard WA, White ER, Dhall R, Cronin SB, Aloni S, et al. Nanoscale temperature mapping in operating microelectronic devices. *Science* (2015) 347:629–32. doi:10.1126/science.aaa2433

14. Menges F, Mensch P, Schmid H, Riel H, Stemmer A, Gotsmann B. Temperature mapping of operating nanoscale devices by scanning probe thermometry. *Nat Commun* (2016) 7:10874. doi:10.1038/ncomms10874

15. Taylor JM, Cappellaro P, Childress L, Jiang L, Budker D, Hemmer PR, et al. High-sensitivity diamond magnetometer with nanoscale resolution. *Nat Phys* (2008) 4:810–6. doi:10.1038/nphys1075

16. Balasubramanian G, Chan IY, Kolesov R, Al-Hmoud M, Tisler J, Shin C, et al. Nanoscale imaging magnetometry with diamond spins under ambient conditions. *Nature* (2008) 455:648–51. doi:10.1038/nature07278

17. Maze JR, Stanwix PL, Hodges JS, Hong S, Taylor JM, Cappellaro P, et al. Nanoscale magnetic sensing with an individual electronic spin in diamond. *Nature* (2008) 455: 644–7. doi:10.1038/nature07279

18. Scheidegger PJ, Diesch S, Palm ML, Degen CL. Scanning nitrogen-vacancy magnetometry down to 350 MK. *Appl Phys Lett* (2022) 120:224001. doi:10.1063/5.0093548

19. Liu G-Q, Feng X, Wang N, Li Q, Liu R-B. Coherent quantum control of nitrogen-vacancy center spins near 1000 kelvin. *Nat Commun* (2019) 10:1344. doi:10.1038/s41467-019-09327-2

20. Wang N, Liu CF, Fan JW, Feng X, Leong WH, Finkler A, et al. Zero-field magnetometry using hyperfine-biased nitrogen-vacancy centers near diamond surfaces. *Phys Rev Res* (2022) 4:013098. doi:10.1103/physrevresearch.4.013098

21. Lenz T, Wickenbrock A, Jelezko F, Balasubramanian G, Budker D. Magnetic sensing at zero field with a single nitrogen-vacancy center. *Quan Sci. Technol.* (2021) 6: 034006. doi:10.1088/2058-9565/abffbd

22. Zheng H, Xu J, Iwata GZ, Lenz T, Michl J, Yavkin B, et al. Zero-field magnetometry based on nitrogen-vacancy ensembles in diamond. *Phys Rev Appl* (2019) 11:064068. doi:10.1103/physrevapplied.11.064068

23. Fortman B, Pena J, Holczer K, Takahashi S. Demonstration of NV-detected ESR spectroscopy at 115 GHz and 4.2 T. *Appl Phys Lett* (2020) 116:174004. doi:10.1063/5.0006014

24. Stepanov V, Cho FH, Abeywardana C, Takahashi S. High-frequency and high-field optically detected magnetic resonance of nitrogen-vacancy centers in diamond. *Appl Phys Lett* (2015) 106:063111. doi:10.1063/1.4908528

25. Aslam N, Pfender M, Stöhr R, Neumann P, Scheffler M, Sumiya H, et al. Single spin optically detected magnetic resonance with 60–90 GHz (E-Band) microwave resonators. *Rev Sci Instrum* (2015) 86:064704. doi:10.1063/1.4922664

26. Doherty MW, Struzhkin VV, Simpson DA, McGuinness LP, Meng Y, Stacey A, et al. Electronic properties and metrology applications of the diamond NV - center under pressure. *Phys Rev Lett* (2014) 112:047601. doi:10.1103/physrevlett.112.047601

27. Dai J-H, Shang Y-X, Yu Y-H, Xu Y, Yu H, Hong F, et al. Optically detected magnetic resonance of diamond nitrogen-vacancy centers under megabar pressures. *Chin Phys. Lett.* (2022) 39:117601. doi:10.1088/0256-307x/39/11/117601

28. Acosta VM, Bauch E, Ledbetter MP, Waxman A, Bouchard L-S, Budker D. Temperature dependence of the nitrogen-vacancy magnetic resonance in diamond. *Phys Rev Lett* (2010) 104:070801. doi:10.1103/physrevlett.104.070801

29. Neumann P, Jakobi I, Dolde F, Burk C, Reuter R, Waldherr G, et al. High-precision nanoscale temperature sensing using single defects in diamond. *Nano Lett* (2013) 13:2738–42. doi:10.1021/nl401216y

30. Toyli DM, de las Casas CF, Christle DJ, Dobrovitski VV, Awschalom DD. Fluorescence thermometry enhanced by the quantum coherence of single spins in diamond. *Proc Natl Acad Sci* (2013) 110:8417–21. doi:10.1073/pnas.1306825110

31. Kucsko G, Maurer PC, Yao NY, Kubo M, Noh HJ, Lo PK, et al. Nanometre-scale thermometry in a living cell. *Nature* (2013) 500:54–8. doi:10.1038/nature12373

32. Dolde F, Fedder H, Doherty MW, Nöbauer T, Rempp F, Balasubramanian G, et al. Electric-field sensing using single diamond spins. *Nat Phys* (2011) 7:459–63. doi:10.1038/nphys1969

33. Michl J, Steiner J, Denisenko A, Bülau A, Zimmermann A, Nakamura K, et al. Robust and accurate electric field sensing with solid state spin ensembles. *Nano Lett* (2019) 19:4904–10. doi:10.1021/acs.nanolett.9b00900

34. Bian K, Zheng W, Zeng X, Chen X, Stöhr R, Denisenko A, et al. Nanoscale electric-field imaging based on a quantum sensor and its charge-state control under ambient condition. *Nat Commun* (2021) 12:2457. doi:10.1038/s41467-021-22709-9

35. Gruber A, Drabenstedt A, Tietz C, Fleury L, Wrachtrup J, von Borczyskowski C. Scanning confocal optical microscopy and magnetic resonance on single defect centers. *Science* (1997) 276:2012–4. doi:10.1126/science.276.5321.2012

36. Rondin L, Tetienne JP, Hingant T, Roch JF, Maletinsky P, Jacques V. Magnetometry with nitrogen-vacancy defects in diamond. *Rep Prog. Phys.* (2014) 77:056503. doi:10.1088/0034-4885/77/5/056503

37. Casola F, Van Der Sar T, Yacoby A. Probing condensed matter physics with magnetometry based on nitrogen-vacancy centres in diamond. *Nat Rev Mater* (2018) 3: 17088. doi:10.1038/natrevmats.2017.88

38. Broadway DA, Johnson BC, Barson MSJ, Lillie SE, Dontschuk N, McCloskey DJ, et al. Microscopic imaging of the stress tensor in diamond using *in situ* quantum sensors. *Nano Lett* (2019) 19:4543–50. doi:10.1021/acs.nanolett.9b01402

39. Kehayias P, Turner MJ, Trubko R, Schloss JM, Hart CA, Wesson M, et al. Imaging crystal stress in diamond using ensembles of nitrogen-vacancy centers. *Phys Rev B* (2019) 100:174103. doi:10.1103/physrevb.100.174103

40. Hsieh S, Bhattacharyya P, Zu C, Mittiga T, Smart TJ, Machado F, et al. Imaging stress and magnetism at high pressures using a nanoscale quantum sensor. *Science* (2019) 366:1349–54. doi:10.1126/science.aaw4352

41. de Lange G, Wang ZH, Ristè D, Dobrovitski VV, Hanson R. Universal dynamical decoupling of a single solid-state spin from a spin bath. *Science* (2010) 330:60–3. doi:10.1126/science.1192739

42. Zhao N, Ho S-W, Liu R-B. Decoherence and dynamical decoupling control of nitrogen vacancy center electron spins in nuclear spin baths. *Phys Rev B* (2012) 85: 115303. doi:10.1103/physrevb.85.115303

43. Yang W, Ma W-L, Liu R-B. Quantum many-body theory for electron spin decoherence in nanoscale nuclear spin baths. *Rep Prog. Phys.* (2017) 80:016001. doi:10.1088/0034-4885/80/1/016001

44. Schäfer-Nolte E, Schlipf L, Ternes M, Reinhard F, Kern K, Wrachtrup J. Tracking temperature-dependent relaxation times of ferritin nanomagnets with a wideband quantum spectrometer. *Phys Rev Lett* (2014) 113:217204. doi:10.1103/physrevlett.113.217204

45. Barry JF, Schloss JM, Bauch E, Turner MJ, Hart CA, Pham LM, et al. Sensitivity optimization for NV-diamond magnetometry. *Rev Mod Phys* (2020) 92:015004. doi:10.1103/revmodphys.92.015004

46. Wolf T, Neumann P, Nakamura K, Sumiya H, Ohshima T, Isoya J, et al. Subpicotesla diamond magnetometry. *Phys Rev X* (2015) 5:041001. doi:10.1103/physrevx.5.041001

47. Zhao Z, Ye X, Xu S, Yu P, Yang Z, Kong X, et al. Sub-nanotesla sensitivity at the nanoscale with a single spin. *Natl Sci Rev* (2023) 10:nwad100. doi:10.1093/nsr/nwad100

48. Wrachtrup J, Finkler A. Hybrid sensors ring the changes. *Nature* (2014) 512: 380–1. doi:10.1038/512380a

49. Choi J, Zhou H, Landig R, Wu HY, Yu X, Von Stetina SE, et al. Probing and manipulating embryogenesis via nanoscale thermometry and temperature control. *Proc Natl Acad Sci* (2020) 117:14636–41. doi:10.1073/pnas.1922730117

50. Fujiwara M, Sun S, Dohms A, Nishimura Y, Suto K, Takezawa Y, et al. Real-time nanodiamond thermometry probing *in vivo* thermogenic responses. *Sci Adv* (2020) 6: eaba9636. doi:10.1126/sciadv.aba9636

51. Simpson DA, Morrisroe E, McCoey JM, Lombard AH, Mendis DC, Treussart F, et al. Non-neurotoxic nanodiamond probes for intraneuronal temperature mapping. *ACS Nano* (2017) 11:12077–86. doi:10.1021/acsnano.7b04850

52. Plakhotnik T, Doherty MW, Cole JH, Chapman R, Manson NB. *All-optical Thermometry and thermal Properties of the optically detected spin Resonances of the NV⁻ Center in nanodiamond. Nano Lett* (2014) 14:4989–96. doi:10.1021/nl501841d

53. Fukami M, Yale CG, Andrich P, Liu X, Heremans FJ, Nealey PF, et al. All-optical cryogenic thermometry based on nitrogen-vacancy centers in nanodiamonds. *Phys Rev Appl* (2019) 12:014042. doi:10.1103/physrevapplied.12.014042

54. Wang N, Liu GQ, Leong WH, Zeng H, Feng X, Li SH, et al. Magnetic criticality enhanced hybrid nanodiamond thermometer under ambient conditions. *Phys Rev X* (2018) 8:011042. doi:10.1103/physrevx.8.011042

55. Zhang T, Liu G-QQ, Leong W-HH, Liu C-FF, Kwok M-HH, Ngai T, et al. Hybrid nanodiamond quantum sensors enabled by volume phase transitions of hydrogels. *Nat Commun* (2018) 9:3188. doi:10.1038/s41467-018-05673-9

56. Liu C-F, Leong W-H, Xia K, Feng X, Finkler A, Denisenko A, et al. Ultra-sensitive hybrid diamond nanothermometer. *Natl Sci Rev* (2021) 8. doi:10.1093/nsr/nwaa194

57. Zhang S-C, Li S, Du B, Dong Y, Zheng Y, Lin H-B, et al. Thermal-demagnetization-enhanced hybrid fiber-based thermometer coupled with nitrogen-vacancy centers. *Opt Mater Express* (2019) 9:4634. doi:10.1364/OME.9.004634

58. Cai J, Jelezko F, Plenio MB. Hybrid sensors based on colour centres in diamond and piezoactive layers. *Nat Commun* (2014) 5:4065. doi:10.1038/ncomms5065

59. Kitagawa R, Nagata S, Arai K, Mizuno K, Tsuji T, Fujisaki I, et al. Pressure sensor using a hybrid structure of a magnetostrictive layer and nitrogen-vacancy centers in diamond. *Phys Rev Appl* (2023) 19:044089. doi:10.1103/physrevapplied.19.044089

60. Li C, Soleyman R, Kohandel M, Cappellaro P. SARS-CoV-2 quantum sensor based on nitrogen-vacancy centers in diamond. *Nano Lett* (2022) 22:43–9. doi:10.1021/acs.nanolett.1c02868

61. Rendler T, Neburkova J, Zemek O, Kotek J, Zappe A, Chu Z, et al. Optical imaging of localized chemical events using programmable diamond quantum nanosensors. *Nat Commun* (2017) 8:14701. doi:10.1038/ncomms14701

62. Fujisaku T, Tanabe R, Onoda S, Kubota R, Segawa TF, So FTK, et al. PH nanosensor using electronic spins in diamond. *ACS Nano* (2019) 13:11726–32. doi:10.1021/acsnano.9b05342

63. Trifunovic L, Pedrocchi FL, Hoffman S, Maletinsky P, Yacoby A, Loss D. High-efficiency resonant amplification of weak magnetic fields for single spin magnetometry at room temperature. *Nat Nanotechnol* (2015) 10:541–6. doi:10.1038/nnano.2015.74

64. Fescenko I, Jarmola A, Savukov I, Kehayias P, Smits J, Damron J, et al. Diamond magnetometer enhanced by ferrite flux concentrators. *Phys Rev Res* (2020) 2:023394. doi:10.1103/physrevresearch.2.023394

65. Xie Y, Yu H, Zhu Y, Qin X, Rong X, Duan C-K, et al. A hybrid magnetometer towards femtotesla sensitivity under ambient conditions. *Sci Bull* (2021) 66:127–32. doi:10.1016/j.scib.2020.08.001

66. Carmiggelt JJ, Bertelli I, Mulder RW, Teepe A, Elyasi M, Simon BG, et al. Broadband microwave detection using electron spins in a hybrid diamond-magnet sensor chip. *Nat Commun* (2023) 14:490. doi:10.1038/s41467-023-36146-3

67. Kolesov R, Grotz B, Balasubramanian G, Stöhr RJ, Nicolet AAL, Hemmer PR, et al. Wave–particle duality of single surface plasmon polaritons. *Nat Phys* (2009) 5:470–4. doi:10.1038/nphys1278

68. Bogdanov SI, Shalaginov MY, Lagutchev AS, Chiang CC, Shah D, Baburin AS, et al. Ultrabright room-temperature sub-nanosecond emission from single nitrogen-vacancy centers coupled to nanopatch antennas. *Nano Lett* (2018) 18:4837–44. doi:10.1021/acs.nanolett.8b01415

69. Chen X-D, Wang E-H, Shan L-K, Feng C, Zheng Y, Dong Y, et al. Focusing the electromagnetic field to 10−6λ for ultra-high enhancement of field-matter interaction. *Nat Commun* (2021) 12:6389. doi:10.1038/s41467-021-26662-5

70. Feng X, Leong WH, Xia K, Liu CF, Liu GQ, Rendler T, et al. Association of nanodiamond rotation dynamics with cell activities by translation-rotation tracking. *Nano Lett* (2021) 21:3393–400. doi:10.1021/acs.nanolett.0c04864

71. McGuinness LP, Yan Y, Stacey A, Simpson DA, Hall LT, Maclaurin D, et al. Quantum measurement and orientation tracking of fluorescent nanodiamonds inside living cells. *Nat Nanotechnol* (2011) 6:358–63. doi:10.1038/nnano.2011.64

72. Rose BC, Huang D, Zhang ZH, Stevenson P, Tyryshkin AM, Sangtawesin S, et al. Observation of an environmentally insensitive solid-state spin defect in diamond. *Science* (2018) 361:60–3. doi:10.1126/science.aao0290

73. Choi S, Agafonov VN, Davydov VA, Plakhotnik T. Ultrasensitive all-optical thermometry using nanodiamonds with a high concentration of silicon-vacancy centers and multiparametric data analysis. *ACS Photon* (2019) 6:1387–92. doi:10.1021/acsphotonics.9b00468

74. Bhaskar MK, Sukachev D, Sipahigil A, Evans R, Burek M, Nguyen C, et al. Quantum nonlinear optics with a germanium-vacancy color center in a nanoscale diamond waveguide. *Phys Rev Lett* (2017) 118:223603. doi:10.1103/physrevlett.118.223603

75. Fan JW, Cojocaru I, Becker J, Fedotov IV, Alkahtani MHA, Alajlan A, et al. Germanium-vacancy color center in diamond as a temperature sensor. *ACS Photon* (2018) 5:765–70. doi:10.1021/acsphotonics.7b01465

76. Widmann M, Lee SY, Rendler T, Son NT, Fedder H, Paik S, et al. Coherent control of single spins in silicon carbide at room temperature. *Nat Mater* (2015) 14:164–8. doi:10.1038/nmat4145

77. Anisimov AN, Simin D, Soltamov VA, Lebedev SP, Baranov PG, Astakhov GV, et al. Optical thermometry based on level anticrossing in silicon carbide. *Sci Rep* (2016) 6:33301. doi:10.1038/srep33301

78. Christle DJ, Klimov PV, de las Casas CF, Szász K, Ivády V, Jokubavicius V, et al. Isolated spin qubits in SiC with a high-fidelity infrared spin-to-photon interface. *Phys Rev X* (2017) 7:021046. doi:10.1103/physrevx.7.021046

79. Lin WX, Yan FF, Li Q, Wang J, Hao ZH, Zhou JY, et al. Temperature dependence of divacancy spin coherence in implanted silicon carbide. *Phys Rev B* (2021) 104:125305. doi:10.1103/physrevb.104.125305

80. Gottscholl A, Kianinia M, Soltamov V, Orlinskii S, Mamin G, Bradac C, et al. Initialization and read-out of intrinsic spin defects in a van Der Waals crystal at room temperature. *Nat Mater* (2020) 19:540–5. doi:10.1038/s41563-020-0619-6

81. Liu W, Li ZP, Yang YZ, Yu S, Meng Y, Wang ZA, et al. Temperature-dependent energy-level shifts of spin defects in hexagonal boron nitride. *ACS Photon* (2021) 8:1889–95. doi:10.1021/acsphotonics.1c00320

82. Stern HL, Gu Q, Jarman J, Eizagirre Barker S, Meng Y, Mendelson N, Chugh D, et al. Room-temperature optically detected magnetic resonance of single defects in hexagonal boron nitride. *Nat Commun* (2022) 13:618. doi:10.1038/s41467-022-28169-z